

# MHD consistent cellular automata (CA) models

## II. Applications to solar flares

H. Isliker<sup>1</sup>, A. Anastasiadis<sup>2</sup>, and L. Vlahos<sup>1</sup>

<sup>1</sup> Section of Astrophysics, Astronomy and Mechanics  
Department of Physics, University of Thessaloniki  
GR 54006 Thessaloniki, GREECE  
isliker@helios.astro.auth.gr, vlahos@helios.astro.auth.gr

<sup>2</sup> Institute for Space Applications and Remote Sensing  
National Observatory of Athens  
GR 15236 Penteli, GREECE  
anastasi@space.noa.gr

Received ...; accepted ...

**Abstract.** In Isliker et al. (2000b), an extended cellular automaton (X-CA) model for solar flares was introduced. In this model, the interpretation of the model's grid-variable is specified, and the magnetic field, the current, and an approximation to the electric field are yielded, all in a way that is consistent with Maxwell's and the MHD equations. The model also reproduces the observed distributions of total energy, peak-flux, and durations. Here, we reveal which relevant plasma physical processes are implemented by the X-CA model and in what form, and what global physical set-up is assumed by this model when it is in its natural state (self-organized criticality, SOC). The basic results are: (1) On large-scales, all variables show characteristic quasi-symmetries: the current has everywhere a preferential direction, the magnetic field exhibits a quasi-cylindrical symmetry. (2) The global magnetic topology forms either (i) closed magnetic field lines around and along a more or less straight neutral line for the model in its standard form, or (ii) an arcade of field lines above the bottom plane and centered along a neutral line, if the model is slightly modified. (3) In case of the magnetic topology (ii), loading can be interpreted as if there were a plasma which flows predominantly upwards, whereas in case of the magnetic topology (i), as if there were a plasma flow expanding from the neutral line. (4) The small-scale physics in the bursting phase represent localized diffusive processes, which are triggered when a quantity which is an approximately linear function of the current exceeds a threshold. (5) The interplay of loading and bursting in the X-CA model can be interpreted as follows: the local diffusivity usually has a value which is effectively zero, and it turns locally to an anomalous value if the mentioned threshold is exceeded, whereby diffusion dominates the quiet evolution (loading), until the critical quantity falls below the threshold again. (6) Flares (avalanches) are accompanied by the appearance of localized, intense electric fields. A typical example of the spatio-temporal evolution of the electric field during a flare is presented. (7) In a variant on the X-CA model, the magnitude of the current is used directly in the instability criterion, instead of the approximately linear function of it. First results indicate that the SOC state persists and is only slightly modified: distributions of the released energy are still power-laws with slopes comparable to the ones of the non-modified X-CA model, and the large scale structures, a characteristic of the SOC state, remain unchanged. (8) The current-dissipation during flares is spatially fragmented into a large number of dissipative current-surfaces of varying sizes, which are spread over a considerably large volume, and which do not exhibit any kind of simple spatial organization as a whole. These current-surfaces do not grow in the course of time, they are very short-lived, but they multiply, giving rise to new dissipative current-surfaces which are spread further around. They show thus a highly dynamic temporal evolution. It follows that the X-CA model represents an implementation of the flare scenario of Parker (1993) in a rather complete way, comprising aspects from small scale physics to the global physical set-up, making though some characteristic simplifications which are unavoidable in the frame-work of a CA.

**Key words.** solar flares, cellular automata, MHD, non-linear processes, chaos, turbulence

## 1. Introduction

There are two approaches to modeling the dynamic evolution of solar flares: Magnetohydrodynamic (MHD) theory and Cellular Automaton (CA) models. MHD represents the traditional physical approach, being based on fluid theory and Maxwell's equations. It gives detailed insight into the small-scale processes in active regions, but it faces problems to model the complexity of entire active regions and solar flares, so that it is usually applied to well-defined, simple topologies, or it is restricted to model only small parts of active regions, often in reduced dimensions (see e.g. Mikic et al. 1989; Strauss 1993; Longcope & Sudan 1994; Einaudi et al. 1996; Galsgaard & Nordlund 1996; Hendrix & Van Hoven 1996; Nordlund & Galsgaard 1997; Dmitruk & Gomez 1998; Galtier & Pouquet 1998; Georgoulis et al. 1998; Karpen et al. 1998; Einaudi & Velli 1999). Global MHD models for solar flares are still in a rather qualitative state. CA models, on the other hand, can rapidly and efficiently treat complexity, i.e. spatially extended, large systems, which consist of many sub-systems (sub-processes), at the price, however, of simplifying strongly the local small-scale processes. Despite this, they are successful in explaining observed statistics of solar flares (the distributions of total energy, peak flux, and durations of observed hard X-ray time-series), giving, however, no information or insight into the small-scale processes (e.g. Lu & Hamilton 1991, Lu et al. 1993, Vlahos et al. 1995, Georgoulis & Vlahos 1996, Galsgaard 1996, Georgoulis & Vlahos 1998; in the following, we will term these models or modifications of them *classical* CA models; a different category of models form the completely stochastic CA models for solar flares (e.g. MacPherson & MacKinnon 1999), which we are not referring to in the following).

The classical CA models were originally derived in analogy to theoretical sand-pile models (Bak et al. 1987; 1988), and despite a vague association of the model's components with physical variables and processes, they had to be considered as basically phenomenological models. Later, Isliker et al. (1998) showed that the basic small-scale processes of the classical CA models can be interpreted as (simplified) MHD processes, for instance loading as strongly simplified shuffling, and redistributing (bursting) as local diffusion processes. However, the classical CA models, even when interpreted in the way of Isliker et al. (1998), show still a number of unsatisfying points from the point of view of MHD: For instance, consistency with MHD and Maxwell's equations is unclear ( $\nabla \mathbf{B}$  can not be controlled), secondary quantities such as currents and electric fields are not available.

In Isliker et al. (2000b; hereafter IAV2000), we introduced the *extended* CA model (hereafter: X-CA model) for solar flares, in which the MHD-inconsistencies are removed, and which is more complete in the sense of MHD than the classical CA models. The X-CA model consists

in the combination of a classical CA model with a set-up which is super-imposed onto the classical CA, and which, concretely, yields the following benefits: (i) The interpretation of the grid-variable is specified, turning the CA models therewith from phenomenological models into physically interpretable ones; (ii) consistency with Maxwell's and the MHD equations is guaranteed, and (iii) all the relevant MHD variables are yielded in a way consistent with MHD: the magnetic field (fulfilling  $\nabla \mathbf{B} = 0$ ), the current, and an approximation to the electric field. The set-up is super-imposable in the sense that it does not interfere with the dynamic evolution (the evolution rules) of the CA model it is super-imposed onto, unless wished. The solar flare X-CA model is able to deal with the complexity of active regions, as are the classical CA models, but its components are now physically interpretable in a consistent way. It represents a realization of plasma-physics (mainly MHD) in the frame of a CA model.

The X-CA model of IAV2000, which uses classical, existing models and extends them, is to be contrasted to the construction of completely new CA models, derived from MHD so that they are compatible with MHD (as for instance the recently introduced CA model of Longcope and Noonan (2000), and the models of Einaudi & Velli (1999), and Isliker et al. (2000a), which moreover are of a non-SOC type).

In IAV2000, some basic properties of the X-CA model (in different variants) in its natural state (self-organized criticality, SOC) were revealed. In particular, it was shown that the observed distributions of total energy, peak-energy, and durations are as well reproduced by the X-CA model as they are by the classical CA models. In this article, our aim is to reveal the global physical set-up and the plasma-physical processes the X-CA model implements and represents when it is in the state of SOC. These physical aspects of the X-CA model will be compared to the flare scenario suggested by Parker (e.g. Parker 1993; see also App. A). We will actually show that the X-CA model may be viewed as an implementation of Parker's (1993) flare scenario.

Differently, we may state the scope of this article as follows: The X-CA model has at its heart a classical, phenomenological CA model, extends it yet and makes it physically interpretable. The X-CA model is thus a physical CA model, contrary to the classical CA models. It is now a posteriori to be seen what physical processes and structures the X-CA actually represents. It did, for instance, not make sense (and actually was impossible) to ask for the magnetic topology implemented by the classical CA models. Now questions like this one make sense, but the answers are not a priori given, and they are not contained in the frame of the classical CA models alone. Also in this sense, the X-CA model represents a true extension of the classical CA models. Moreover, it is a priori not clear that the physical properties of the X-CA model we are going to reveal are compatible with what is believed to happen physically in flares, just the statistical results are known to be compatible with the observations. The

results of this article will yet show that the X-CA model can indeed be considered as making physically sense in the context of the flare modeling problem, it may be viewed as a reasonable *physical* model for flares, all the more with the modifications we will introduce.

The questions concerning the implemented plasma-physical processes and global physical set-up we address in this article are (Sec. 3): (1) what the magnetic topology in SOC state represents, (2) what the loading process actually simulates, (3) what physical small-scale processes are implied by the model's energy release events, (4) how the electric field evolves in space and time during flares. More-over, in Sec. 4, the X-CA model is modified to be closer to the flare scenario of Parker by using directly the current in the instability criterion. Lastly, it will be shown how the regions of current-dissipation, which appear during flares, are organized in space and time (Sec. 5). We will start by giving a short summary of the X-CA model (Sec. 2).

## 2. Short summary of the extended CA (X-CA) model

The extended CA (X-CA) model, whose detailed description is given in IAV2000, uses a 3-D cubic grid and the local vector-potential  $\mathbf{A}_{ijk} = \mathbf{A}(\mathbf{x}_{ijk})$  at the grid-sites  $\mathbf{x}_{ijk}$  as the primary grid-variable. In order to calculate derivatives of the vector-potential, the latter is made a continuous function in the entire modeled volume by interpolating it with 3-D cubic splines. In this way, the magnetic field is determined as  $\mathbf{B} = \nabla \wedge \mathbf{A}$ , and the current as  $\mathbf{J} = \frac{c}{4\pi} \nabla \wedge \mathbf{B}$ , both as derivatives of  $\mathbf{A}$  and according to MHD. The electric field is approximated by the resistive term of Ohm's law in its simple form,  $\mathbf{E} = \eta \mathbf{J}$  (see the discussion of this approximation in Sec. 3.4), where the diffusivity  $\eta$  is given as  $\eta = 1$  at the bursting sites and zero everywhere else (following the analysis of Isliker et al. (1998); see also Sec. 3.3).

As a measure of the stress  $\mathbf{S}_{ijk}$  in the primary field  $\mathbf{A}_{ijk}$  we use two alternative definitions: (i) in Sec. 3 the classical or *standard* form  $\mathbf{S}_{ijk} \equiv d\mathbf{A}_{ijk} := \mathbf{A}_{ijk} - \frac{1}{n_n} \sum_{n,n.} \mathbf{A}_{n,n.}$  (where the sum is over the first order nearest neighbours of the central point, and  $n_n$  is the number of these neighbours), following Lu & Hamilton (1991) and most of the classical CA models; and (ii), in Secs. 4 and 5, taking advantage of the availability of secondary variables in the X-CA model, we use the current as a stress measure,  $\mathbf{S}_{ijk} \equiv \mathbf{J}_{ijk}$ , which is physically more sensible than the standard  $d\mathbf{A}_{ijk}$  (see the discussion in Sec. 4).

The grid-variable  $\mathbf{A}$  undergoes two different regimes of dynamic evolution, loading (quiet evolution) and bursting (redistributing): During loading, random vector-field increments  $\delta\mathbf{A}_{ijk}$  are dropped at random grid-sites. If locally the magnitude of the stress  $\mathbf{S}_{ijk}$  exceeds a threshold then the system starts bursting: The vector-field is redistributed among the unstable site and its nearest neighbours ( $\mathbf{A}_{ijk} \rightarrow \mathbf{A}_{ijk} - n_n/(n_n + 1) \mathbf{S}_{ijk}$  for the central

unstable grid-point, and  $\mathbf{A}_{nn} \rightarrow \mathbf{A}_{nn} + 1/(n_n + 1) \mathbf{S}_{ijk}$  for its nearest neighbours). The amount of energy released in one burst is estimated as Ohmic dissipation,  $E_{burst} \sim \eta \mathbf{J}^2$  with, as stated,  $\eta = 1$  at bursting sites (for details see Eq. (10) in IAV2000).

The model shows a transient phase before reaching a stationary state, the state of self-organized criticality (SOC), in which avalanches (flares) of all sizes occur, with power-law distributions of total energy, peak energy and durations, which agree as well with the corresponding observed distributions as do the distributions yielded by the classical CA models (see IAV2000).

One of the necessary conditions for the system to reach the state of SOC is that the loading increments  $\delta\mathbf{A}_{ijk}$  exhibit a preferred spatial directionality (see e.g. Lu & Hamilton (1991)). The used preferred direction can be freely chosen, it does not change the statistical results of the model. In Sec. 3, it will yet turn out that the used preferred direction influences the magnetic topology. We will investigate two preferred directions: (a) parallel to the spatial diagonal of the simulation cube, as used in all the classical CA models, and ultimately following the original prescription of Lu & Hamilton (1991). We call this the *standard* preferred direction. (b) We will use the  $x$ -direction as preferred direction of loading.

The magnetic topology depends also on the boundary conditions (b.c.) applied around the simulation cube; actually it is the combination of the b.c. with the preferred direction of the loading increments which determines the magnetic topology, as will be shown in Sec. 3. We will apply two different kinds of b.c.: (1) open b.c. (together with the standard preferred direction of the loading increments), as introduced by Lu & Hamilton (1991) and used (most likely) in all the classical CA models, which we call thus the *standard* b.c. (2) We will apply open b.c. around the simulation box except at the lower ( $x$ - $y$ ) boundary plane, where we will assume closed b.c. (in combination with the preferred loading direction along the  $x$ -axis). In App. B, the details of our implementation of open and closed b.c. are described.

## 3. The physical processes and global physical set-up implemented by the extended CA model

### 3.1. The global topology of the magnetic field and of the current

In IAV2000, it was demonstrated that the solar flare X-CA model exhibits a characteristic large scale organization of  $|\mathbf{B}|$ , the magnitude of the magnetic field, whereas the magnitude of the current,  $|\mathbf{J}|$ , seems not to exhibit any obvious large scale-organization. The question we address here is what these structures represent and whether they can be identified with structures in observed active regions.

The X-CA model makes magnetic field-lines available: through the continuation (interpolation, see Sec. 2), the vector-potential is given also in-between grid-sites, hence

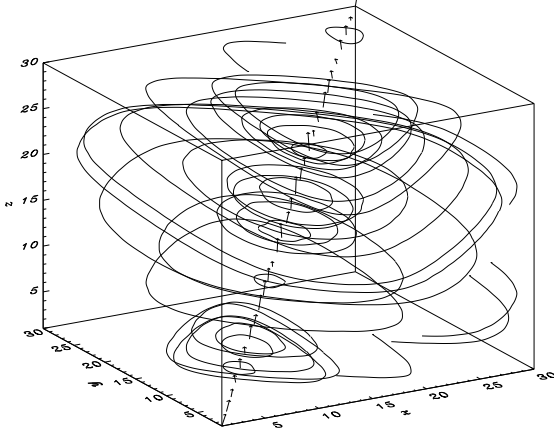


**Fig. 1.** Magnetic field lines yielded by the X-CA model in its standard form, originating from randomly selected points. The vectors along the diagonal represent the (rescaled) currents (off-diagonal currents are not shown). Near the diagonal a neutral line is situated.

also its derivatives, and therewith as well the magnetic field (see IAV2000 for more details). Magnetic field-lines at a fixed time can then be constructed as usual by integrating along the continuously given magnetic field, starting from some initial point.

### 3.1.1. The quasi-symmetries and their origin

A typical single magnetic field line in the simulation box of the X-CA model in its standard form (see Sec. 2), which starts at an arbitrary point, winds itself around the diagonal and closes on itself, or it leaves the modeled cube. In Fig. 1, a number of field lines is shown, starting from randomly chosen points in the simulation box (at an arbitrary, fixed time in the loading phase during the SOC state, and for a grid-size  $30 \times 30 \times 30$ ). The magnetic field obviously shows cylindrical quasi-symmetry.

Fig. 1 also shows the currents at the diagonal (the currents at the other grid-sites are not shown for purposes of better visualization): they are preferentially aligned with the diagonal, and this preferential direction is actually exhibited everywhere in the simulation box and at all times during SOC-state, so that also the current shows a quasi-symmetry.

The reason for these quasi-symmetries is the quasi-symmetry imposed on the primary grid-variable by the loading rule: The loading increments are asymmetric, namely with preferential direction parallel to the diagonal (Sec. 2). Since the bursting rules are isotropic and symmetric in the three components of  $\mathbf{A}$ , the vector potential  $\mathbf{A}$  maintains the quasi-symmetry of the loading increments and is preferentially aligned with the diagonal (parallel to  $(1, 1, 1)$ ). As a result of this quasi-symmetry of the vector-potential, the magnetic field ( $\sim \nabla \wedge \mathbf{A}$ ) and the current ( $\sim \nabla \wedge \mathbf{B}$ ) must exhibit the mentioned sym-

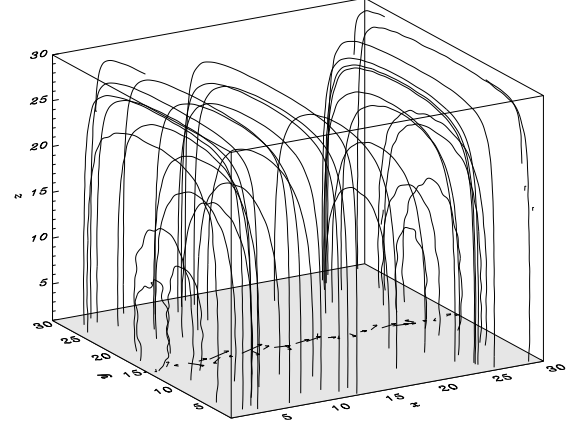


**Fig. 2.** Magnetic field lines yielded by the modified X-CA model (see Sec. 3.1.2), originating from randomly selected points. The vectors shown in the shaded bottom plane represent the local (rescaled) currents (the currents at the other grid-sites are not shown). A neutral line is situated very roughly along the shown currents.

metries: If we introduce cylindrical coordinates, with the  $z'$ -axis along the diagonal of the cube and  $r$  the perpendicular distance from the  $z'$ -axis, then, in obvious notation, due to its quasi-symmetry  $\mathbf{A}$  reduces to  $\mathbf{A} \approx A_{z'}(r) \mathbf{e}_{z'}$ , from where it follows that  $\mathbf{B}$  must be of the form  $\mathbf{B} = \nabla \wedge \mathbf{A} \approx -\frac{\partial A_{z'}}{\partial r} \mathbf{e}_\phi$  (all the other terms vanish), and finally for  $\mathbf{J}$  we get  $\mathbf{J} = \frac{c}{4\pi} \nabla \wedge \mathbf{B} \approx -\frac{c}{4\pi} \frac{1}{r} \frac{\partial}{\partial r} \left( r \frac{\partial A_{z'}}{\partial r} \right) \mathbf{e}_{z'}$ .

A consequence of these quasi-symmetries is that the current is always and everywhere more or less perpendicular to the magnetic field, though in general with a small parallel component, since the symmetries are always slightly distorted.

### 3.1.2. The magnetic field topology

In the standard form of the X-CA model, the magnetic field is obviously described by quasi-cylindrically symmetric, closed field-lines around a more or less straight neutral line, which follows roughly the diagonal, as shown in Fig. 1.

A second, different magnetic topology is formed by the X-CA model in its non-standard form, where we let the preferential direction of the loading increments be along the  $x$ -direction, and we apply closed boundary conditions at the lower boundary (the  $x$ - $y$ -plane), keeping though all the other boundaries open (see Sec. 2).

The field lines form now an arcade above the bottom (shaded)  $x$ - $y$ -plane (Fig. 2), centered along a more or less straight neutral line in this plane (which follows very roughly the currents shown in Fig. 2 — note that, as in Fig. 1, only a subset of the currents is shown, for better visualization). If we interpret the shaded  $x$ - $y$ -plane as the photosphere, then the picture is reminiscent of an arcade of loops.

The effect of the modifications on the magnetic topology can be explained as follows: The new preferred directionality of the loading increments causes the neutral line (the symmetry axis) to be parallel to the  $x$ -axis, and to go through the mid-point of the grid (the argumentation is analogous to the one in Sec. 3.1.1). The new boundary condition at the bottom plane causes the symmetry axis (neutral line) to move down into the bottom  $x$ - $y$ -plane, so that the field lines open and leave the simulation box through the bottom plane.

We just note that the statistical results the X-CA model yields in this modification are still compatible with the observations (power-law distributions of peak-flux and total flux, with indices of roughly 1.8 and 1.4, respectively, i.e. the SOC state persists).

### 3.2. What the loading process simulates

The interpretation of the loading process depends on the magnetic topology. Let us first consider the variant of the X-CA model where the magnetic field forms an arcade of field lines, as in Fig. 2 (Sec. 3.1.2). The vector-potential  $\mathbf{A}$  in coronal applications is in general assumed to evolve according to

$$\frac{\partial \mathbf{A}}{\partial t} = \mathbf{v} \wedge \mathbf{B} + \eta \frac{c^2}{4\pi} \nabla^2 \mathbf{A} - \eta \frac{c^2}{4\pi} \nabla(\nabla \mathbf{A}) + \nabla \chi, \quad (1)$$

which is the integrated induction equation of MHD, and where  $\eta$  is the diffusivity and  $\chi$  an arbitrary function. The loading process' role is to mimic the quiet evolution of active regions, i.e., according to Parker's flare scenario, the shuffling of the magnetic field due to random foot-point motions (see App. A). In terms of MHD, this implies that the convective term in Eq. (1) governs the temporal evolution. Let us thus assume that the loading increments  $\delta \mathbf{A}$  represent perturbations due to this convective term, i.e.  $\delta \mathbf{A} \sim (\mathbf{v} \wedge \mathbf{B})$  (from Eq. 1), so that the loading process implicitly implements the effect of a plasma with velocity  $\mathbf{v}$ . Since the increments of loading  $\delta \mathbf{A}$  are preferentially along the  $x$ -axis (see Sec. 3.1.2), and since  $\mathbf{B}$  is from left to right in Fig. 2 — note the preferential direction of the currents near the neutral line —, the direction of  $\mathbf{v}$  follows from the relation  $\delta \mathbf{A} \sim (\mathbf{v} \wedge \mathbf{B})$  as being from the neutral line radially up- and outwards (radial in the sense of being perpendicular to the neutral line). The sketch in Fig. 3 illustrates the situation. Thus, the preferential direction of the loading can obviously be interpreted as if there were a plasma which flows predominantly upwards, out of the shaded  $x$ - $y$ -plane in Fig. 2 (see also Fig. 3).

In case of the X-CA model in its standard form, the magnetic topology (closed magnetic field lines around a straight neutral line, as in Fig. 1) would imply, by the same argumentation as before, that the loading must be considered as if there were a plasma expanding perpendicularly away from the neutral line, symmetrically into all radial directions.

In conclusion, the loading increments  $\delta \mathbf{A}$  can be interpreted as being parallel to  $\mathbf{v} \wedge \mathbf{B}$ , with  $\mathbf{v}$  the velocity of an

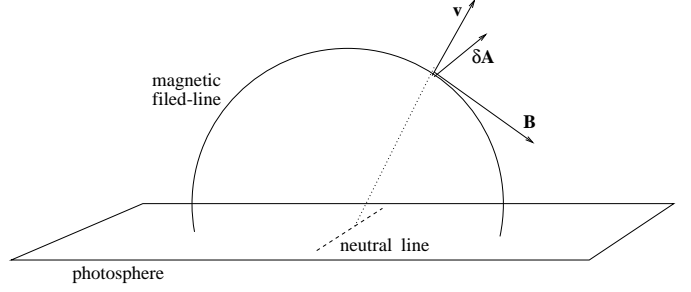


**Fig. 3.** Sketch to illustrate the loading process: the loading increments  $\delta \mathbf{A}$  can be considered as being proportional to  $\mathbf{v} \wedge \mathbf{B}$ , with  $\mathbf{v}$  the velocity of the implicitly assumed plasma, and  $\mathbf{B}$  the magnetic field.

assumed up- or out-flowing plasma, respectively, and, as a consequence, the direction of  $\delta \mathbf{A}$  depends on the direction of  $\mathbf{B}$ , the pre-existing magnetic field (not, however, on  $|\mathbf{B}|$ , the magnitude of  $\mathbf{B}$ ). — Note that this interpretation is valid only in SOC state, when the magnetic field has organized itself into its characteristic large-scale structure.

### 3.3. Small scale processes: bursts

Isliker et al. (1998) have shown that the redistribution (burst) rules we use (see Sec. 2) can be interpreted as  $\mathbf{A}$  evolving in the local neighbourhood of an unstable site according to the simple diffusion equation

$$\frac{\partial \mathbf{A}}{\partial t} = \eta \nabla^2 \mathbf{A}, \quad (2)$$

with the boundary condition  $(\mathbf{n} \cdot \nabla) \mathbf{A} = 0$  around the local neighbourhood, and with diffusivity  $\eta = 1$ . It is important to stress, however, that the X-CA redistribution rules for  $\mathbf{A}$  do not represent the discretized version of Eq. (2), but they represent the transition *in one time step* from a given initial local field to the asymptotic solution of Eq. (2) (see Isliker et al. 1998). The time-step  $\Delta t$  of the X-CA model therewith is roughly the diffusive time, and the grid-spacing  $\Delta h$  is roughly the diffusive length scale (as the value of the diffusivity, the numerical values of  $\Delta t$  and  $\Delta h$  are not specified and set to one).

The evolution of  $\mathbf{A}$  according to Eq. (2) in the X-CA corresponds exactly to what the induction equation of MHD (Eq. 1) is expected to reduce to for the case of anomalous diffusion in cylindrical symmetry: (a) According to Parker's flare scenario, the diffusivity at unstable sites is anomalous, i.e. increased by several orders of magnitude (see App. A), so that the convective term can be assumed to be negligible in the induction equation. (b) The quasi-symmetry of the vector-potential (Sec. 3.1.1) implies that  $\mathbf{A}$  is of the form  $\mathbf{A} \approx A_z(r) \mathbf{e}_z$  (by using the same cylindrical coordinate system as in Sec. 3.1.1), so that  $\nabla \mathbf{A} \equiv (1/r) \partial / \partial r (r A_r) + (1/r) \partial A_\phi / \partial \phi + \partial A_z / \partial z \approx 0$ , and therewith  $\nabla(\nabla \mathbf{A}) \approx 0$  in the induction equation.

The most characteristic simplifications made by the X-CA model are: (i) The boundary conditions are unre-

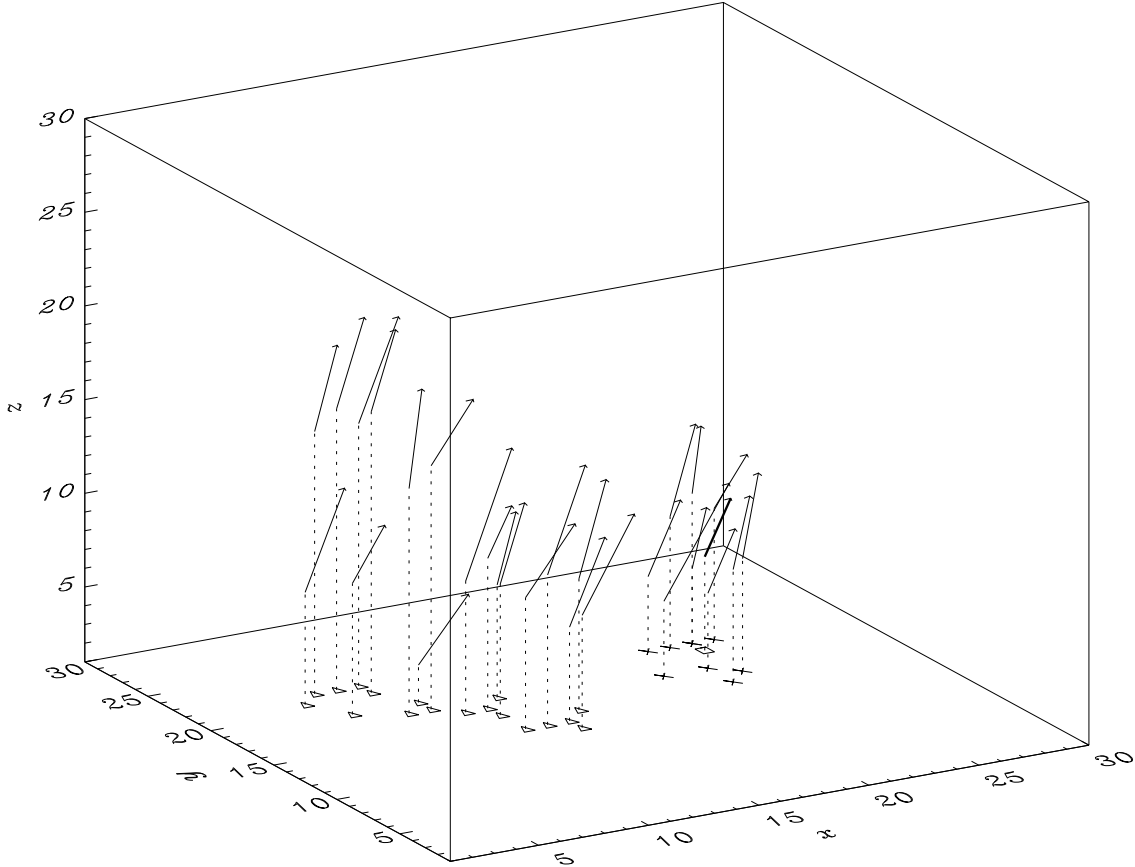


**Fig. 4.** The electric field-vectors during a flare, at three different time-steps: at the beginning of the flare (bold-vector, projected grid-site in  $x$ - $y$ -plane marked with a rectangle); after nine time-step (marked with 'x'); after 91 time-steps (marked with triangles). The vectors are shown in 3-D parallel projection, rescaled for visualization purposes, with length proportional to  $|\mathbf{E}|$ . Note that the electric fields of three different time-steps are shown together for visualization purposes, in the model actually only one set appears at a time, the fields of the previous time-steps have become zero again, at later times.

alistically simple. They actually imply that  $\int_{n.n.} \mathbf{A} dV$  is conserved in the diffusion events (see Isliker et al. 1998). (ii) All the diffusion events have the same diffusivity, diffusive length scale and diffusive time.

The amount of energy released in the diffusion events of the X-CA model is determined through the expression for Ohmic dissipation (see Sec. 2), following directly the MHD prescription.

Lastly, we turn to the instability criterion of the X-CA model in its standard form (the non-standard instability criterion is discussed in Sec. 4): Bursts occur in the model if the local stress ( $|d\mathbf{A}_{ijk}|$ ) exceeds a threshold (see Sec. 2)). In IAV2000, it has been shown that there, where the stress  $|d\mathbf{A}_{ijk}|$  exceeds the threshold, also  $|\mathbf{J}_{ijk}|$  is increased, and after a burst both  $|d\mathbf{A}_{ijk}|$  and  $|\mathbf{J}_{ijk}|$  are relaxed. Actually,  $|\mathbf{J}_{ijk}|$  is an approximately linear function of  $|d\mathbf{A}_{ijk}|$  for large enough  $|d\mathbf{A}_{ijk}|$ , monotonically increasing with  $|d\mathbf{A}_{ijk}|$  (see IAV2000). This is very reminiscent of Parker's flare scenario (see App. A): During the load-

ing phase, a diffusivity  $\eta = 0$  is assumed everywhere. If a threshold in the stress, which is a linear function of the current, is reached somewhere, then  $\eta = 1$  in the local neighbourhood, and diffusion sets on. As in Parker's flare scenario, the diffusivity thus assumes anomalous values (one), if a linear function of the current reaches a certain threshold. Otherwise it is small (ordinary) and effectively set to zero.

### 3.4. The electric field

Of particular interest is the electric field in the X-CA model, since it is the cause for particle acceleration and the associated non-thermal radiation of flares. In the X-CA model, the electric field is approximated by the resistive term of Ohm's law in its simple form,  $\mathbf{E} = \eta \mathbf{J}$  (Sec. 2), which can be expected to be a good approximation, since in the applications we are interested in events of current dissipation. This argument is actually based on Parker's

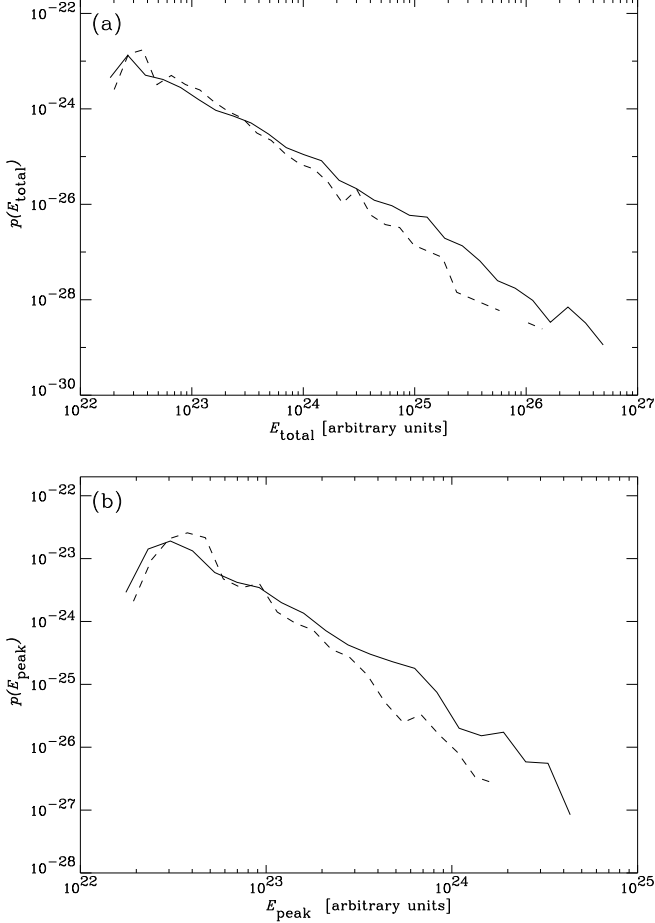


**Fig. 5.** Probability distribution of total energy (a) and peak flux (b) for the X-CA model in its standard form according to Sec. 2 (solid), and using the current in the instability criterion and in the redistribution rules, see Sec. 4 (dashed). The energy units are arbitrary.

flare scenario (see App. A), together with the assumption that Ohm's law in its simple form is a reasonable approximation in coronal active regions: the diffusivity is small at most times in active regions (build-up phase, loading phase), and the simple Ohm's law for the electric field ( $\mathbf{E} = \eta \mathbf{J} - \frac{1}{c} \mathbf{v} \wedge \mathbf{B}$ ) reduces to  $\mathbf{E} = -\frac{1}{c} \mathbf{v} \wedge \mathbf{B}$ . However, if the diffusivity becomes anomalous at a bursting site, as described in App. A, and increases by several orders of magnitude, then the electric field must be expected to be dominated by the resistive part,  $\mathbf{E} = \eta \mathbf{J}$ , and it is this contribution to the electric field which will be the cause of particle acceleration during flares. We thus assume in our applications the  $\mathbf{E}$ -field usually to be zero (assuming in the non bursting phase the velocities to be small and therewith the electric field to be negligible), and only if the instability criterion is fulfilled at some grid-sites, an electric field of the form  $\mathbf{E} = \eta \mathbf{J}$  appears for one time-step. If the burst is over (in the following time-step, and if the site does not again fulfill the instability criterion), the electric field is zero again.

In Fig. 4, the electric field as it appears during a flare (avalanche) in the SOC state of the X-CA model is illustrated (for a  $30 \times 30 \times 30$ -grid): We chose a medium-size flare, which lasted 181 time-steps. In the figure, the electric field is shown for three different time steps in the course of the flare: At the onset of the flare, one grid-site is unstable, and it carries an electric field, whereas all the other grid-sites have a zero electric field. After nine time-steps, the instabilities have traveled away from the initially unstable site and are spread around it, and the electric field appears correspondingly at these sites. After 91 time-steps, the unstable sites are spread over a larger volume, which is not surrounding the initial site anymore, the instabilities have traveled to a different region in the grid, where the corresponding electric fields appear.

Remarkably, the electric-fields which appear are all of comparable intensity, and they are all more or less along the same preferential direction. The former is due to the fact that the current is an approximately linear function of  $d\mathbf{A}$  for large values of  $d\mathbf{A}$ , as stated earlier (see IAV2000 for details), which itself is just above the threshold, so that through the relation  $\mathbf{E} = \eta \mathbf{J}$  all the electric field magnitudes are similar. The parallelity is due to the quasi-symmetry obeyed by the current in the SOC state (Sec. 3.1.1): the current is preferentially along the diagonal of the cubic grid, and as a consequence of the relation  $\mathbf{E} = \eta \mathbf{J}$ , the electric field has the same preferential direction.

Likewise, the electric field is always more or less perpendicular to the magnetic field, exhibiting though in general a small parallel component. This is again a consequence of the relation  $\mathbf{E} = \eta \mathbf{J}$  and of the corresponding property of the current (see Sec. 3.1.1).

#### 4. A modification of the extended CA model: the current as the critical quantity

One difference between the X-CA model in its standard form and Parker's flare scenario is that the current  $|\mathbf{J}_{ijk}|$  is not directly used as a critical quantity (see App. A), but rather  $|d\mathbf{A}_{ijk}|$  (see Sec. 2 and the discussion in Sec. 3.3). This leads us to modify the X-CA model, and to use as the stress measure  $\mathbf{S}$  directly the current  $\mathbf{J}$  (see Sec. 2). The new instability criterion is

$$|\mathbf{J}_{ijk}| > J_{cr}. \quad (3)$$

(with  $J_{cr} = f \frac{c}{4\pi} A_{cr}$ , where  $f$  is chosen from Fig. 4 of IAV2000 such that the threshold  $A_{cr}$  for  $|\mathbf{J}_{ijk}|$  corresponds roughly to the threshold for  $|d\mathbf{A}_{ijk}|$ ). Redistribution events in this variant can thus directly be considered as representing current driven instabilities. The use of  $\mathbf{J}_{ijk}$  instead of  $d\mathbf{A}_{ijk}$  also in the redistribution rules is motivated through the following argument: the use of  $d\mathbf{A}_{ijk}$  can be justified by Eq. (2), which is hidden behind the bursts in the X-CA model, since  $d\mathbf{A}_{ijk}$  is an approximation to  $\nabla^2 \mathbf{A}$  (see IAV2000). However, since the in-

duction equation (Eq. 1), when neglecting the convective term, can equivalently be written as

$$\frac{\partial \mathbf{A}}{\partial t} = -\eta c \mathbf{J} + \nabla \chi, \quad (4)$$

it is more natural from the point of view of MHD to use  $\mathbf{J}_{ijk}$  also in the redistribution rules. The result of these modifications is (using a grid-size  $30 \times 30 \times 30$ ) that according to first results the SOC state persists, with power-law distributions (Fig. 5) which are a bit steeper (5% to 10%), and a large scale structure of the magnetic field which is very close to the one of the non-modified X-CA model (see Sec. 3.1, and IAV2000).

We just note that when using  $\mathbf{J}_{ijk}$  only in the instability criterion, but not in the redistribution rules (where still  $d\mathbf{A}_{ijk}$  is used), it turns out that sooner or later the model finds itself in an infinite loop, independent of the value of  $J_{cr}$ . The reason is that  $|\mathbf{J}_{ijk}|$  is an approximately linear function of  $|d\mathbf{A}_{ijk}|$  only for large stresses  $|d\mathbf{A}_{ijk}|$ , but the opposite is not true, there are cases where  $|\mathbf{J}_{ijk}|$  is large but  $|d\mathbf{A}_{ijk}|$  is almost zero (see IAV2000 for details). In these cases, a burst should happen ( $|\mathbf{J}_{ijk}|$  is large), but the almost zero  $d\mathbf{A}_{ijk}$  cannot redistribute the fields, and the algorithm falls into an endless loop.

## 5. The spatial organization of the current-dissipation regions

Before turning to flares, it is worthwhile to illustrate how the spatial regions of intense, but sub-critical current are spatially organized during the quiet evolution (loading) of the X-CA model, since any structures the current forms in the quiet evolution are the base on top of which the flares take place. A three-dimensional representation of the surfaces of constant current-density at a sub-critical level ( $|\mathbf{J}| = \text{const.} = 9.1 \cdot 10^{10}$ ) is shown in Fig. 6, for an arbitrary time during the loading phase in the SOC-state (i.e. no grid-sites are unstable in the figure), as given by the X-CA model in the version of Sec. 4. The current in the entire simulation box ranges from  $0.1 \cdot 10^{10}$  to  $12.0 \cdot 10^{10}$ , and the threshold is  $J_{cr} = 12.02 \cdot 10^{10}$  (the units are arbitrary). The current-density obviously organizes itself into a large number of current surfaces of varying sizes, all smaller though than the modeled volume, and homogeneously distributed over the simulation box. The numerical values of the current densities span a range until just very little below the threshold, which is actually typical for the loading phase, and consequently the system can easily become unstable at some grid-site through further loading.

Of particular interest is the spatial structure of the unstable regions during flares, i.e. of the regions of current-dissipation (see Sec. 3.3), whether and how these regions are spatially organized, and also how one spatial structure emerges from the immediately previous one. In Fig. 7, the regions of current-dissipation are shown for two different time-steps during a flare (i.e. the surfaces of  $|\mathbf{J}| = J_{cr} \equiv 12.02 \cdot 10^{10}$ , which enclose the regions where

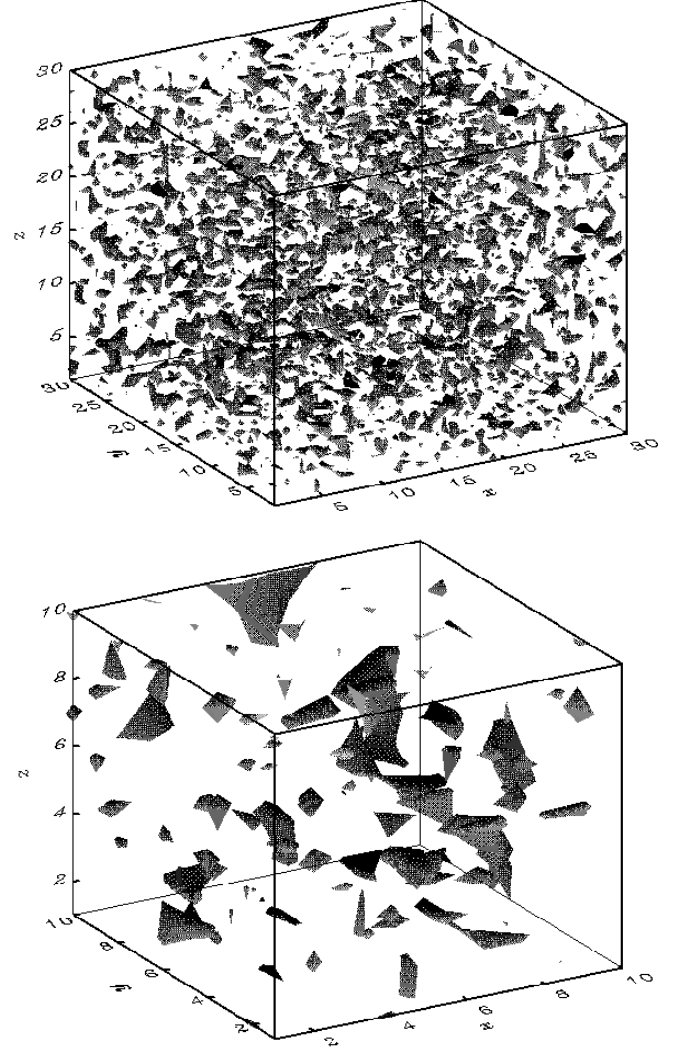


**Fig. 6.** Three-dimensional representation of the (shaded) surfaces of constant (sub-critical) current-density ( $|\mathbf{J}| = 9.1 \cdot 10^{10}$ ) at an arbitrary time during the loading phase, in the entire simulation box (top panel), and zoomed (bottom panel).

the current is above the threshold): A flare starts with one single, usually very small, region of super-critical current. This small region does not grow, but multiplies in its neighbourhood, it gives rise to spreading of unstable regions, i.e. of current-dissipation regions. The secondary regions of current-dissipation multiply again, etc., and after not too many time-steps the appearing current-dissipation regions become numerous and vary in size, the larger ones having the shape of current surfaces, as in Fig. 7 (top panels), which is at an early stage in the flare. These current-surfaces multiply further and travel through the grid, giving rise now to even larger numbers of current surfaces, as in Fig. 7 (bottom panels), which is at a later time, during the main phase of the flare. The degree of fragmentation has increased, and the current surfaces are spread now over a considerable volume. The picture in Fig. 7 (bottom panels) is typical for a flare of intermediate duration (the



flare lasted 177 time-steps) as far as the size of the largest current surfaces, the degree of fragmentation, and the spatial dispersion are concerned, though the concrete picture continuously changes in the course of time. Towards the end of the flare, the current surfaces tend to become less numerous, and finally they die out quickly.

## 6. Summary, Discussion and Conclusions

### 6.1. Summary

The extended CA (X-CA) model, introduced in IAV2000, is consistent with Maxwell's and the magnetic part of the MHD equations, and makes all the secondary variables (currents, electric fields) available. In IAV2000, it was shown that the X-CA model (in different variants) reproduces as well as the classical CA models the observed distributions of total flux, peak-flux, and durations, and that it can be considered as a model for energy release through current-dissipation, which was confirmed here and supported with more facts. In this article, our aim was to reveal the small-scale physics and the global physical set-up implemented by the X-CA model when it is in the SOC state. The basic results are:

**1. Quasi-symmetries of all the grid variables:** A consequence of the SOC state are the characteristic quasi-symmetries of the fields: preferential alignment with the cube-diagonal for the vector potential and the current, and cylindrical quasi-symmetry around the diagonal for the magnetic field (for the model in its standard form).

**2. Magnetic field topology:** For the preferred directionalities of loading and boundary conditions adopted here, the global topology of the magnetic field has two varieties: either it forms an arcade of magnetic field lines, centered along a neutral line for the modified X-CA model, or it forms closed magnetic field lines around and along a more or less straight neutral line for the model in its standard form.

**3. Interpretation of the loading process:** In the variant of the model where the magnetic field forms an arcade of field lines above a bounding surface which includes a neutral line, loading can be considered as if there were a plasma which flows upwards from the neutral line. In the variant of the model where the magnetic field consists in closed field lines along a neutral line, loading can be considered as if there were a plasma which expands away from the neutral line.

**4. Small scale processes (bursts):** The redistribution events occurring at unstable sites can be considered as localized diffusion processes, accompanied by energy release through current-dissipation. The diffusion is accomplished in one-time step, going from the initial state directly to the asymptotic solution of a simple diffusion equation. The diffusivities, diffusive length-scales and diffusive times are the same for all bursts.

**5. Spatio-temporal evolution of the electric field:** The X-CA model yields the spatio-temporal evolution of

the intense and localized electric fields, which appear at the sites of current-dissipation during flares. Typically, the electric fields are of similar magnitude and similar direction, and the locations where they appear travel through the grid in the course of time.

**6. The current as the critical quantity:** A modification which brings the X-CA model closer to Parker's flare scenario and plasma physics is the replacement of the standard stress measure with the current, so that directly a large current is responsible for the occurring of a burst. First results indicate that the SOC state basically persists under this modification, the large scale structure of the magnetic field remains the same, the distributions of total and peak energy remain power-laws, with a slight tendency towards steepening.

**7. The nature of the instability criterion and the diffusivity:** The local diffusion events start if a locally defined stress exceeds a threshold. This local stress corresponds either to an approximately linear function of the current for large stresses (in the standard version of the X-CA model; see Sec. 3.3), or directly to the current (in the version of Sec. 4). The X-CA model thus implicitly implements Parker's flare scenario that an instability is triggered if the current  $J$  (or a linear function of it) exceeds some threshold, with the result that the resistivity increases and diffusion dominates the time evolution. Physically, one would think of the diffusion to become anomalous; in the X-CA model the resistivity switches locally from zero to one during one time-step.

**8. Global organization of the current-dissipation regions:** The current-dissipation is spatially and temporally fragmented into a large number of practically independent, dispersed, and disconnected dissipation regions with the shape of current-surfaces, which vary in size and are spread over a considerable volume. These current-surfaces do not grow in the course of time, but they multiply and are short-lived.

### 6.2. Discussion

The magnetic topology in the X-CA model (Sec. 3.1.2) has to be compared to the current picture we have of a flaring active region, where the field topology is complex, with structures on all scales, and with no simple organization of the entire flaring region. A judgment of the X-CA model's magnetic field topology depends on what part of an active region one intends to describe. If we assume or intend to model entire active regions or substantial parts of them, then we would naturally prefer the variant of the X-CA model where the magnetic field forms an arcade of field lines (Fig. 2). Qualitatively, the picture the model gives is not bad, though the observations show a still higher degree of complexity (more than one, and non-straight neutral lines, etc.). Moreover, it seems unlikely that well separated, isolated loops can be identified in the model's magnetic field structure. These two discrepancies should preferably be interpreted as simplifications

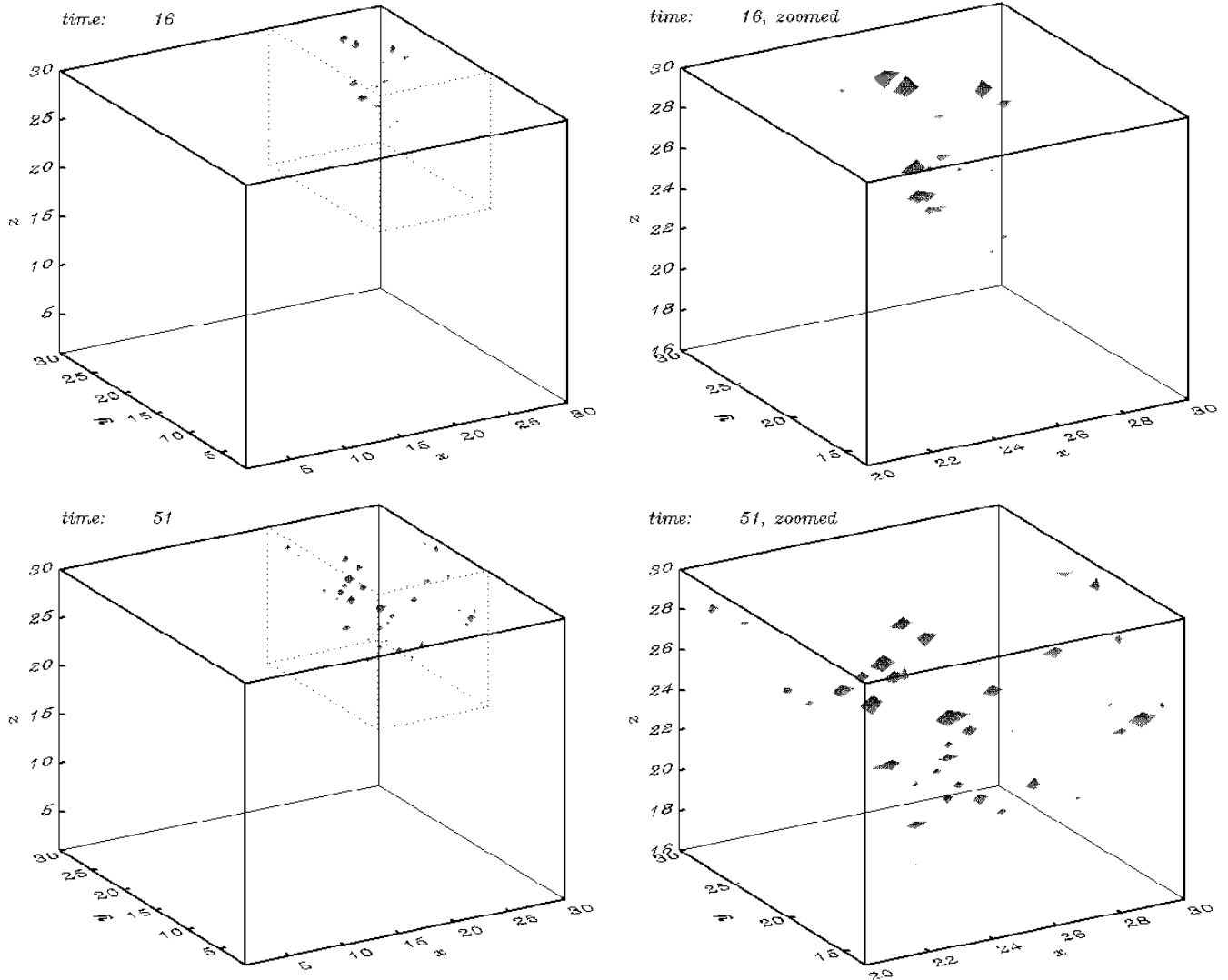


**Fig. 7.** Three-dimensional representation of the current-dissipation regions appearing during a flare, i.e. of the (shaded) surfaces of constant current-density equal to the threshold ( $|\mathbf{J}| = J_{cr} = 12.02 \cdot 10^{10}$ ), for different times during a flare: at time-step 16 after the beginning (top-panels, left: the entire simulation box, right: zoom of the dotted region), and at time-step 51 (bottom-panels, left: the entire simulation box, right: zoom of the dotted region).

the model makes — although, they alternatively might also be interpreted in the way that the magnetic topology represents only a part of an active region, or even just the inner part of one single loop. However, this second interpretation would just open new questions of adequacy, which replace the discussed ones.

More difficult to judge is what the magnetic field topology of the standard variant of the model, the closed field-lines along a straight neutral line (Fig. 1), might correspond to. Such structures are not observed, so that they would have to correspond to small-scale structures, below today’s observational capabilities. We might, for instance, assume that these structures are the X-CA model’s representation of an eddy of three-dimensional MHD turbulence.

The variant of the X-CA model which yields the arcade of field lines has physically more realistic boundary

conditions (closed boundaries at the bottom plane; Secs. 2 and 3.1.2) than the standard form (open boundaries at the bottom plane), if we assume the bottom plane to represent the photosphere: Coronal flares (avalanches) may propagate out of the simulation cube in all directions, assuming that we are not modeling the entire corona, they should, however, not propagate freely into the photosphere, where the physical conditions are strongly different from the ones in the corona, but they should rather leave the photospheric magnetic field basically unchanged. Note that the discussed boundary conditions are relevant in our model (as well as in the classical CA models) only for the bursts, not though for loading, which we discuss next.

The loading process has the interesting interpretation that it implicitly assumes a velocity field which systematically flows upwards against the arcade of magnetic field-lines (or expands the closed field lines, in the case of the

other magnetic topology), which is very reminiscent of the realistic scenario of newly emerging, upwards moving flux, pushing against the already existing magnetic flux and causing in this way occasional magnetic diffusion events, i.e. events of energy release (Sec. 3.2). Despite this interesting interpretation, the loading process is still unsatisfyingly simplified: (a) The loading increments  $\delta \mathbf{A}$  do depend on the direction of the pre-existing magnetic field (see Sec. 3.2), but they should also depend on the magnitude of  $\mathbf{B}$  if one assumes them to represent disturbances according to the  $\mathbf{v} \wedge \mathbf{B}$  term of the induction equation. (b) The loading process acts everywhere and independently in the entire simulation box, whereas according to Parker's flare scenario (see App. A), it should act independently only on one boundary of the simulation box and propagate from there into the system, since an active region is driven only from one boundary, the photo-sphere, (by random foot-point motions and newly emerging flux), from where perturbations propagate along the magnetic field-lines into the active region. We just note that also all the more or less different loading processes of the classical CA models suffer from the problems (a) and (b). A velocity field was explicitly introduced into a CA so far only by the CA model of Isliker et al. (2000a), which is, however, a non-classical CA model, with evolution rules directly derived from MHD.

An interesting property — or prediction — of the X-CA model is the preferred directionality of the appearing currents and electric fields, parallel to the neutral line (Secs. 3.1.1, 3.4). Since both the currents and the electric fields are only indirectly observable, this prediction is difficult to verify with observations. The length-scale over which the currents and electric fields are parallel depends on what part of an active region the X-CA model actually represents.

It is also worthwhile noting that the currents are everywhere more or less perpendicular to the magnetic field (Sec. 3.1.1), and therewith the magnetic field in the physical set-up of the X-CA model is not force-free, opposite to what is usually assumed in MHD for the coronal plasma in its quiet evolution. As the current, so is the electric field always more or less perpendicular to the magnetic field, having in general, though, a small parallel component (Sec. 3.4).

The model's diffusive small-scale physics in the burst mode represents quite well anomalous diffusive processes, despite some characteristic simplifications (Sec. 3.3). The most peculiar assumption made in the X-CA model is the conservation law for the vector-potential ( $\int \mathbf{A} dV = \text{const.}$ ), which holds during bursts and which is a necessary condition for the X-CA model, as for the classical CA models, to reach the SOC state (see e.g. Lu & Hamilton 1991; Lu et al. 1993). As a consequence, also  $\int \mathbf{B} dV$  is conserved during bursts. The physical meaning of this conservation law seems unclear: in MHD, for instance, not directly  $\int \mathbf{A} dV$  or  $\int \mathbf{B} dV$  are expected to be conserved, but  $\int \mathbf{A} \mathbf{B} dV$ , the magnetic helicity (if the

integration volume is chosen adequately; see e.g. Biskamp 1997).

The regions of intense, but sub-critical current-density in the quiet evolution of the X-CA model are organized in current surfaces of various sizes (Sec. 5). A similar picture, though with characteristic differences (e.g. with much less fragmentation), has been reported in the 3-D MHD simulations of coronal plasmas by Nordlund and Galsgaard (e.g. 1997). The pictures yielded by the X-CA model and by the MHD simulations are different not least due to the fact that the MHD simulations have high spatial resolution, and they model a smaller volume than the X-CA model does, so that, among others, the current surfaces in the X-CA model are spatially less resolved, they are smaller, and they do not reach the size of the entire simulation box as they do in the MHD simulations.

The current-dissipation regions at any time during a flare in the X-CA model do not show any sign of global spatial organization between them, and they can definitely not be considered as the dissipation and destruction of a well defined, simple structure (as for instance the disruption of a single, extended current-sheet would be). Moreover, the energy dissipation shows a highly dynamic spatio-temporal behaviour: The current-dissipation regions are not statically maintained at fixed grid-sites during a flare (as it would be the case if they were continuously fed with in-streaming plasma), but they are short lasting and travel through the grid, exploring the near-to-unstable regions. As a consequence, the volume participating in the energy release process is considerably large at most times during a flare, a flare in the X-CA model is never a localized process. Lastly, note that all the ever changing current-dissipation regions which participate in a flare carry their own, independent magnetic field-lines, which are rooted in the photosphere (in the variant of the model with the magnetic field topology in the form of an arcade, Fig. 2).

Finally, it is worthwhile noting an essential difference between MHD simulations and the X-CA model: MHD simulations do not so far invoke anomalous resistivity. In MHD simulations,  $\eta$  is given a fixed and constant numerical value (which moreover is usually adjusted to the grid-size for numerical reasons). The X-CA model, on the other hand, incorporates the kinetic plasma physics which rules the behaviour of the resistivity  $\eta$ , simulating the effect of occasionally appearing anomalous resistivities due to current instabilities (see Sec. 3.3). As all the classical CA models, it can so far not model current dissipation in the frame of a constant, ordinary diffusivity as the result of the interplay of shears in the magnetic field and the velocity field. A complete model for solar flares should ultimately incorporate both dissipation mechanisms.

Due to this difference, a comparison of the current-dissipation regions of the X-CA model in the flaring phase to MHD simulations seems not realistic.

### 6.3. Conclusions

The X-CA model represents an implementation of Parker's (1993) flare scenario, covering aspects from small-scale plasma physics and MHD to the large scale physical set-up and magnetic topologies: most aspects are in good accordance with Parker's flare scenario, even though some give rise to ambiguous interpretations with associated open questions, and some involve unsatisfying simplifications which need improvement. One should be aware that CA models, which by definition evolve according to rules in a discrete space and in discrete time-steps, have by their nature to make simplifications, and one cannot expect them to give exactly the same picture as the observations or MHD simulations, one can just demand that the simplifications are adequate and reasonable, that the over-all picture is as close as possible to the physical one, and, of course, that the quantitative results they give (e.g. concerning energy release) are in good accordance with the observations.

The X-CA model allows different future applications and questions which could not be asked so far in the frame of classical CA models, and it gives more or refined results. One application is a more detailed comparison of the X-CA model to observations. For instance, particles can now be introduced into the model, their thermal radiation can be monitored, and they can be accelerated through the electric fields to yield non-thermal emission (e.g. synchrotron emission; an earlier study of particle acceleration in a classical CA model was made by Anastasiadis et al. (1997), who had to estimate the electric field still indirectly). Very promising on the side of the X-CA model is that the energy dissipation is fragmented and spread over a considerably large volume, with a large number of dissipation regions, so that particle acceleration in the frame of the X-CA model can be expected to be very efficient.

An important property of the X-CA model is not least its flexibility, which allows to implement concrete plasma-physical or MHD ideas in the frame-work of a CA. This was demonstrated here and in IAV2000 by several modifications: the direct use of the current in the instability criterion, the energy release in terms of Ohmic dissipation, and by the modifications which led to a more realistic magnetic topology.

*Acknowledgements.* We thank K. Tsiganis and M. Georgoulis for many helpful discussions on several issues. We also thank G. Einaudi for stimulating discussions on MHD aspects of flares, and the referee A.L. MacKinnon for discussions on several aspects of CA and MHD, and for his critics which helped to improve this article. The work of H. Isliker was partly supported by a grant of the Swiss National Science Foundation (NF grant nr. 8220-046504).

### Appendix A: Short summary of Parker's flare scenario

The flare scenario of Parker (e.g. 1993) can briefly be summarized as follows (whereby also a few basic obser-

vational facts concerning flares and active regions shall be mentioned): Active regions are characterized by a highly complex magnetic topology, with sub-structures on a large variety of scales (e.g. Bastian & Vlahos 1997, Bastian et al. 1998). Generally, in an active region the diffusivity  $\eta$  is small (the magnetic Reynolds number is much larger than unity), and convection dominates the evolution of the magnetic field, i.e. the magnetic field is built-up and continuously shuffled due to random photospheric foot-point motions (the magnetic fields are ultimately rooted in the turbulent convection zone). In this way, magnetic energy is stored in active regions. Occasionally, magnetic structures with high shear may locally be formed, in which the current is increased. If the current is intense enough, then it is expected from plasma-physics that a kinetic instability is triggered, most prominently the ion-acoustic instability. This instability causes in turn the diffusivity  $\eta$  of the plasma to become locally anomalous and therewith to increase drastically (by several orders of magnitude, see e.g. references in Parker (1993)). The evolution of the magnetic field is then governed *locally* by diffusion, convection is negligible. In these local diffusion processes, energy is released due to Ohmic dissipation with a rate  $\eta J^2$ , until the free energy is more or less dissipated and the current has fallen to a much smaller value, so that also  $\eta$  returns to its ordinary value. In flares, such local diffusion events (bursts) appear in a large number during a relatively short period of time, spread over this time-interval and in space, and releasing in their sum considerable amounts of energy. Flares are thus considered to be fragmented into many sub-events, and there is some kind of chain-reaction or domino-effect, whose exact form is an open problem of flare modeling (CA models for instance consider a domino-effect to be operating).

### Appendix B: Open and closed boundary conditions

The boundary conditions (b.c.) around the simulation cube affect the redistribution rules and the definition of the stress measure  $\mathbf{S}_{ijk}$ . In case of open b.c., an implicit layer of zero-field around the grid is assumed, held constant during the entire time-evolution. The numerical factor  $n_n$  in the definition of  $d\mathbf{A}_{ijk}$  and in the redistribution rules (see Sec. 2) has a fixed value,  $n_n = 6$ , assuming that every grid point has six nearest neighbours (the grid we use is cubic), independent of whether it is at the boundaries or not. Consequently, in the definition of  $d\mathbf{A}_{ijk}$  the sum has always six terms, the  $\mathbf{A}_{nn}$  outside the grid contributing zero. The continuation method which is used to determine  $\mathbf{B}$  and  $\mathbf{J}$  explicitly takes the zero-layer around the grid into account (see IAV2000).

In the case of closed b.c., no communication takes place between the field in the grid and the region outside the grid. The definition of  $d\mathbf{A}$  is adjusted to  $d\mathbf{A} = \mathbf{A} - 1/m_n \sum' \mathbf{A}_{nn}$ , where the primed sum is now only over the nearest neighbours which are *inside* the grid, and  $m_n$  is the number of these interior nearest neighbours ( $m_n$

can thus be less than 6). The continuation method does not assume any layer of pre-fixed field around the grid in order to determine  $\mathbf{B}$  and  $\mathbf{J}$ . The redistribution rules are formally the same as introduced in Sec. 2, just that again  $n_n$  is replaced by  $m_n$ , the effective number of nearest neighbours inside the grid.

As stated in Sec. 2, we use two version of b.c., one where all the boundaries are open, and a mixed b.c., with open boundaries at all the boundary planes except for a closed boundary at the lower  $x$ - $y$  plane, i.e. we assume a layer of zero-field around the grid and take it into account, except at the lower boundary, which is treated differently, as described above.

## References

- Anastasiadis, A., Vlahos, L., Georgoulis, M., 1997, Ap. J. 489, 367  
 Bak, P., Tang, C., Wiesenfeld, K., 1987, Phys. Rev. Lett. 59, 381  
 Bak, P., Tang, C., Wiesenfeld, K., 1988, Phys. Rev. A 38, 364  
 Bastian, T. S., Benz, A. O., Gary, D. E., 1998, Ann. Rev. of Astron. & Astrophys. 36, 131  
 Bastian, T.S.; Vlahos, L., 1997, in Coronal Physics from Radio and Space Observations, Lecture Notes in Physics 483, ed. Trottet, G. (Springer-Verlag, Berlin), p. 68  
 Biskamp, D., 1997, Nonlinear Magnetohydrodynamics, Cambridge University Press, Cambridge  
 Bromund, K. R., McTiernan, J. M., Kane, S. R., 1995, Ap. J. 455, 733  
 Dmitruk, P., Gomez, D.O., 1998, Ap. J. 505, 974  
 Einaudi, G., Velli, M., Politano, H., Pouquet, A., 1996, Ap. J. 457, L13  
 Einaudi, G., Velli, M., 1999, Physics of Plasmas 6 (No. 11), 4146  
 Galsgaard, K., 1996, A&A 315, 312  
 Galsgaard, K., Nordlund, A., 1996, J. Geophys. Res. 101, 13445  
 Galtier, S., Pouquet, A., 1998, Sol. Phys. 179, 141  
 Georgoulis, M., Velli, M., Einaudi, G., 1998, Ap. J. 497, 957  
 Georgoulis, M., Vlahos, L., 1996, Ap. J. 469, L135  
 Georgoulis, M., Vlahos, L., 1998, A&A 336, 721  
 Hendrix, D.L., Van Hoven, G., 1996, Ap. J. 467, 887  
 Isliker, H., Anastasiadis, A., Vassiliadis, D., Vlahos, L., 1998, A&A 335, 1085  
 Isliker, H., Anastasiadis, A., Vlahos, L., 2000a, in The Fourth Astronomical Conference of The Hellenic Astronomical Society, eds. Seimenis, J. et al., in press  
 Isliker, H., Anastasiadis, A., Vlahos, L., 2000b, A&A 363, 1134 [IAV2000]  
 Karpen, J.T., Antiochos, S.K., Devore, C. R., Golub, L., 1998, Ap. J. 495, 491  
 Longcope, D.W., Noonan, E.J., 2000, Ap. J. 542, 1088  
 Longcope, L., Sudan, L., 1994, Ap. J. 437, 491  
 Lu, T.E., Hamilton, R.J., 1991, Ap. J. 380, L89  
 Lu, T.E., Hamilton, R.J., McTiernan, J.M., Bromund, K.R., 1993, Ap. J. 412, 841  
 MacPherson, K.P., MacKinnon, A.L., 1999, A&A 350, 1040  
 Mikic, Z., Schnack, D.D., Van Hoven, G., 1989, Ap. J. 338, 1148  
 Nordlund, A. Galsgaard, K., 1997, in Proc. 8th European Solar Physics Meeting, Lecture Notes in Physics 489, eds. G. Simnett, C. E. Alissandrakis, and L. Vlahos, Springer, Heidelberg, p. 179  
 Parker, E.N., 1993, Ap. J. 414, 389  
 Strauss, H., 1993, Geophys. Res. Lett. 20, 325  
 Vlahos, L., Georgoulis, M., Kluiving, R., Paschos, P., 1995, A&A 299, 897